THE JOURNAL OF PHYSICAL CHEMISTRY C
A JOURNAL OF THE AMERICAN CHEMICAL SOCIETY

pubs.acs.org/JPCC Article

Oxidative Stability of $Nb_{n+1}C_nT_z$ MXenes

Ian J. Echols, Dustin E. Holta, Vrushali S. Kotasthane, Zeyi Tan, Miladin Radovic, Jodie L. Lutkenhaus, and Micah J. Green*

Cite This: J. Phys. Chem. C 2021, 125, 13990−13996

Read Online

ACCESS | Metrics & More | Article Recommendations | Supporting Information

ABSTRACT: Despite prior reports on oxidation and oxidation mitigation for $Ti_{n+1}C_nT_z$ MXenes, there have been no reports on the oxidative stability of MXene dispersions outside of this family to date, including Nb-based MXenes. Here, we monitor the oxidative stability of $Nb_{n+1}C_nT_z$ MXenes by using UV−vis absorbance and XPS and demonstrate methods to mitigate oxidation. We show that the inclusion of an antioxidant (i.e., ascorbic acid) and low temperature storage improve the oxidative stability of $Nb_{n+1}C_nT_z$ MXenes. We also demonstrate that MXenes with higher "*n*" are more oxidatively stable. Our results suggest that the use of an antioxidant and low temperature storage may be generalized for improving the oxidative stability of all MXenes outside of the $Ti_{n+1}C_nT_z$ family. This discovery shows potential for the future use of new MXenes and that MXenes with higher "*n*" are more favorable for long-term storage and use.

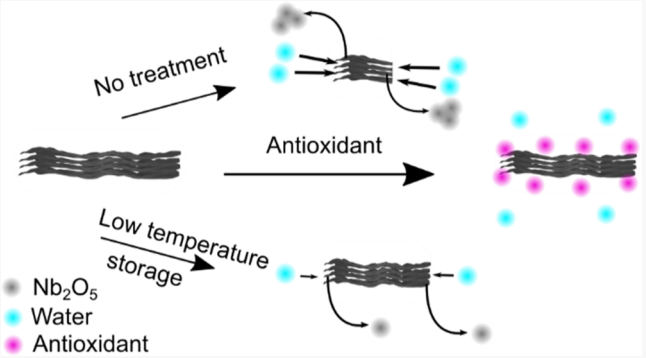

INTRODUCTION

Despite the widespread interest in MXenes with compositions beyond the Ti family, little is known about the colloidal and oxidative stability of Nb-based MXenes. MXenes are a class of 2D nanomaterials with numerous possible compositions owing to the ability to vary both the M and X elements of the parent MAX phase with Nb-based MXenes being among the possible compositions that have been successfully synthesized.[1,2] Although numerous MXenes have been theoretically predicted to exist, only a fraction has been experimentally synthesized to date.[2] MXenes have the chemical formula $M_{n+1}X_nT_z$ and are obtained by selectively etching the 'A' element from a MAX phase precursor where M is a transition metal, A is a group 13 to 16 element, X is either carbon or nitrogen, T is a surface terminal group, and *n* is 1, 2, or 3. By changing the M and X components, a broad range of electrical and optical properties can be obtained, enabling the use of MXenes in a wide variety of applications (e.g., energy storage, sensing, catalysis, and EMI shielding).[3−9] Despite the wide variety of possible MXenes, most studies to date have been focused on $Ti_3C_2T_z$. More recently, Nb-based MXenes have drawn increasing interest.[10−12]

However, the shelf life of MXenes is significantly hindered by their poor oxidative stability, which makes it difficult to use them in a number of devices, and in the case of $Nb_{n+1}C_nT_z$ MXenes, the shelf life has not been reported to date.[13−16] Previous studies by Zhang et al. demonstrated that colloidal dispersions of $Ti_3C_2T_z$ oxidize completely within days.[14] The poor oxidative stability of $Ti_3C_2T_z$ was also observed by Lee et al. for MXene films.[15] Oxidation of the MXene results in the conversion of the MXene to its respective metal oxide accompanied by a significant reduction in conductvity.[13]

As such, a number of methods have been explored to improve the oxidative stability of MXenes.[13−15,17−19] Initial studies explored storage at low temperatures and in inert environments such as Ar.[14,18] Unfortunately, these storage conditions are not always feasible when using MXenes in devices. More recently, our group has demonstrated that the use of antioxidants can significantly improve the shelf life of $Ti_3C_2T_z$.[17,20] The effectiveness of this method has already been demonstrated for their respective MXene-based films.[6] In this case, films assembled with antioxidant-treated $Ti_3C_2T_z$ were less prone to oxidation as compared to those assembled without an antioxidant. Although a number of studies have explored the oxidation of $Ti_3C_2T_z$ MXenes, the oxidation of $Nb_{n+1}C_nT_z$ MXene dispersions is yet to be studied. Palisaitis et al. had previously shown that the Nb/O ratio of Nb_2CT_z MXenes will decrease over time, indicating oxidation.[21] However, this study was done using drop-cast films as opposed to dispersions. As new MXenes are synthesized and their possible applications are explored, it is critical to expand these oxidation studies to new MXenes.

Received: February 4, 2021
Revised: May 27, 2021
Published: June 16, 2021

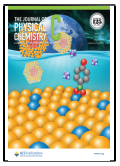

https://doi.org/10.1021/acs.jpcc.1c01064
J. Phys. Chem. C 2021, 125, 13990−13996

Here we report, for the first time, on the oxidation stability of $Nb_{n+1}C_nT_z$ MXenes in aqueous dispersions and demonstrate methods to improve their shelf lives. The two methods evaluated in this work are low-temperature storage and the addition of an antioxidant, specifically ascorbic acid, to verify if these methods are applicable to MXenes outside of the $Ti_{n+1}C_nT_z$ family. We then compare the oxidative stability of $Nb_{n+1}C_nT_z$ MXenes with different n values. Similar to previous reports for Ti_3C_2 MXenes, UV−vis absorbance of $Nb_{n+1}C_nT_z$ dispersions was used as a metric for the degree of oxidation.[14] We then use a first-order reaction model to assess the oxidation reaction kinetics.

METHODS

$Nb_{n+1}AlC_n$ MAX phases were synthesized by pressureless sintering in a 50 mm alumina tube vacuum furnace (MTI Corp.). First, Nb (325 mesh, 99.8%, Alfa Aesar), Al (325 mesh, 99%, Alfa Aesar), and graphite (7−11 μm, 99%, Alfa Aesar) elemental powders were mixed at 300 rpm for 24 h using 35 mm diameter zirconia cylinders in a jar rolling mill. Atomic ratios of Nb/Al/C = 2:1.1:0.95 and Nb/Al/C = 4:1.5:2.7 were used for Nb_2AlC and Nb_4AlC_3, respectively. The mixed powders were then loaded into alumina crucibles for sintering in the tube furnace. The tube furnace was evacuated using a two-pump vacuum system and backfield with ultra-high purity Ar (UHP Ar). Sintering was completed at 1600 °C for Nb_2AlC and 1650 °C for Nb_4AlC_3 under flowing UHP Ar with a dwell time of 4 h. The samples were then allowed to cool under ambient conditions to room temperature and were then ground with an alumina mortar and pestle and sieved to obtain 20−45 μm particle size distribution.

Similar to previous reports, $Nb_{n+1}C_nT_z$ was obtained by selectively etching Al from the parent MAX phase using HF (48−51%, Alfa Aesar).[22,23] 20 mL of stock HF was added into a 100 mL polypropylene beaker with a lid. Holes were drilled in the lid to prevent gas buildup during etching. 1 g of the MAX phase powder was slowly added to the etching container over 5 min to mitigate overheating due to the exothermic reaction. MAX phase powders were then etched for 90 and 118 h for Nb_2AlC and Nb_4AlC_3, respectively, at room temperature with constant stirring. After etching, excess HF was removed by centrifugal solvent exchange with DI water at 9000 rpm for 20 min. Washes were repeated until the pH of the decanted solution reached ∼ 6.

The obtained $Nb_{n+1}C_nT_z$ clay was dispersed in 25 mL of 20 wt % tetrabutylammonium hydroxide (TBAOH, 40 wt %, Sigma-Aldrich) in water per gram of the starting MAX phase and left to intercalate for 8 h with constant stirring. Excess TBAOH was removed by two centrifugal solvent exchanges with milli-Q water at 10,000 rpm for 20 min. The intercalated clay was then bath-sonicated in an ice bath for 60 min to delaminate the expanded clay. The final MXene supernatant was then obtained by centrifuging the bath-sonicated dispersion for 30 min at 3500 rpm and collecting the supernatant. Dispersion concentration was initially determined using vacuum-assisted filtration (VAF) with a 0.1 μm pore size filter paper. UV−vis absorbance of the same supernatant was measured at varying concentrations using a Shimadzu SolidSpec-3700 UV−vis−NIR spectrophotometer. Using the concentrations determined from VAF, an extinction coefficient was determined for both MXenes and UV−vis absorbance was used to measure the concentration of all other MXene supernatants. L-ascorbic acid (AA, 99%, Sigma-Aldrich) was added to dispersions at a concentration of 1 mg/mL, if indicated.

Samples for SEM (scanning electron microscopy, JEOL JSM-7500F), XRD (Bruker-AXS Advanced Bragg−Brentano X-ray powder diffractometer), and XPS (X-ray photoelectron spectroscopy, Omicron XPS/UPS system with Argus detector) were prepared by VAF of the as-prepared MXene supernatant. All samples were stored under vacuum before characterization. Detailed constraints for XPS deconvolution can be found in the Supporting Information. The samples for dynamic light scattering (DLS) and ζ potential measurements (Malvern Zetasizer Nano ZS) were prepared by diluting the as-prepared dispersions to ∼0.05 mg/mL.

To quantify the degree of oxidation, UV−vis absorbance of MXene dispersions was taken at varying storage times. UV−vis of MXene dispersions was measured using spectrophotometry (Shimadzu SolidSpec-3700 UV−vis−NIR spectrophotometer). All samples were redispersed by hand shaking prior to measurements. In between measurements, the samples were left undisturbed. All samples were baselined using milli-Q water and scans were taken from 300 to 800 nm. Equation 1 was then used to fit the experimental data and quantify the oxidative stability of each of the samples as[14]

$$A = A_0 + A_1 \exp(-t/\tau) \quad (1)$$

where A is the absorbance, A_0 and A_1 are the constants, t is the storage time, and τ is the reaction timescale. The ratio of A_1 to $A_0 + A_1$ indicates the fraction of the sample that is prone to oxidation. Standard error for the model fitting constants was calculated in MATLAB using a 95% confidence interval.

XPS of MXenes before and after aging were also compared to evaluate the degree of oxidation. Nb_2CT_z and $Nb_4C_3T_z$ dispersions were allowed to age for 2 weeks. For each MXene, dispersions were aged under two different conditions, either at RT without AA or at 15 °C with AA, to compare the expected extremes. After aging, the samples were vacuum-filtered and dried under vacuum prior to XPS measurements.

RESULTS & DISCUSSION

Nb_2CT_z and $Nb_4C_3T_z$ MXenes were synthesized by the selective etching of Al from their respective MAX phase precursors similar to previous reports.[22,23] The detailed procedure can be found in the Supporting Information. The final solid in the supernatant was then used for further characterization and to determine the oxidative stability. The colloidal stability of the dispersions was then assessed visually by the Tyndall effect. Figure 1a,b shows the Tyndall effect occurring in $Nb_{n+1}C_nT_z$ aqueous dispersions (∼0.05 mg/mL). The visible laser throughout the sample indicates colloidal stability of the dispersion.

The as-prepared aqueous dispersions were then prepared into films using VAF. X-ray diffractograms of VAF films (Figure 1c) indicated that a downshift in 2θ occurred after etching. This indicates successful removal of Al from the MAX phase and thereby successful etching. From the positions of the (002) peaks in XRD, the respective d-spacings in the Nb_2CT_z and $Nb_4C_3T_z$ MXene films can be calculated and increased from 0.7 to 1.1 nm and 1.2 to 1.5 nm, respectively, after etching. The presence of some non-basal peaks is attributed to the presence of multilayers which can be seen in top-down SEM images of the vacuum-filtered films (Figure 1d,e).

X-ray photoelectron spectroscopy was then used to verify the composition of the $Nb_{n+1}C_nT_z$ MXenes. Samples for XPS

https://doi.org/10.1021/acs.jpcc.1c01064
J. Phys. Chem. C 2021, 125, 13990−13996

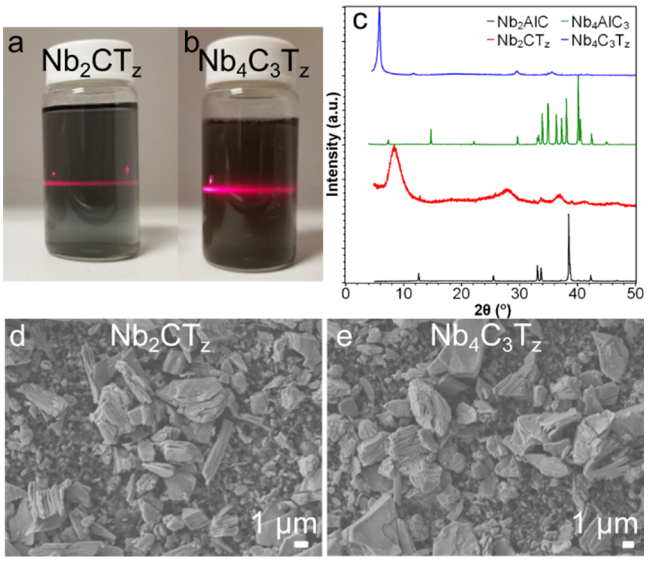

Figure 1. Colloidal dispersions of (a) Nb_2CT_z and (b) $Nb_4C_3T_z$. (c) XRD of $Nb_{n+1}C_nT_z$ MXenes and their respective MAX phase precursors. Top-down SEM images of vacuum-filtered (d) Nb_2CT_z and (e) $Nb_4C_3T_z$ supernatants. MXene samples for XRD were prepared by VAF. MAX phase powders were used as prepared for XRD.

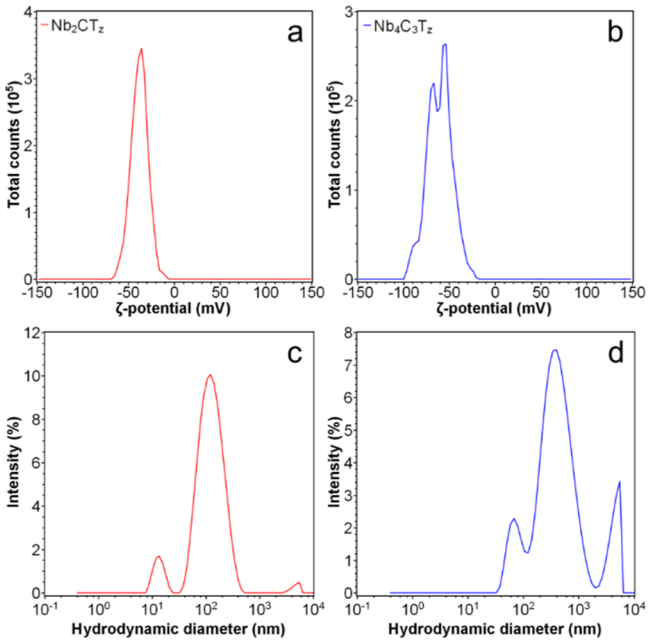

Figure 2. ζ potential distribution of (a) Nb_2CT_z and (b) $Nb_4C_3T_z$ dispersions. Hydrodynamic size distribution of (c) Nb_2CT_z and (d) $Nb_4C_3T_z$ dispersions. Dispersion concentrations were ~0.05 mg/mL.

were prepared by VAF of the solid in the supernatant. Survey scans of both VAF MXene films (Figure S1) indicated the presence of all expected components (Nb 3d, C 1s, O 1s, and F 1s). The absence of a peak for Al 2p indicated the removal of Al and confirmed successful etching. Component spectra were then deconvoluted following previous reports (Figures S2 and S3)[22] and detailed peak fitting results are provided in Tables S1 and S2. The presence of surface terminal groups (−OH, −F, and −O) was confirmed for both MXenes. Additionally, Nb (I, II, IV) and Nb* peaks are present in the Nb 3d spectra, confirming successful MXene synthesis. Although oxide peaks are apparent in both the starting MXene dispersions, this is likely caused by the oxidation of the MXenes during the processing procedure after etching. Processing lasts several hours and during this time the MXenes are exposed to an oxidizing environment, leading to the formation of the oxide peak in XPS.

SEM (Figure 1d,e) was then employed to assess the surface morphology of the vacuum-filtered $Nb_{n+1}C_nT_z$ films. For both Nb_2CT_z and $Nb_4C_3T_z$ films prepared by VAF of the solid in the supernatant, well-exfoliated nanosheets were visible along with few-layer nanosheets.

ζ potentials of the $Nb_{n+1}C_nT_z$ dispersions at ~0.05 mg/mL (Figure 2a,b) were then measured to assess the colloidal stability. The pH of the as-prepared dispersions was ~6 and was not adjusted. No antioxidant was used at this point. The measured ζ potentials were −38.0 ± 9.2 and −60.3 ± 15.9 mV for Nb_2CT_z and $Nb_4C_3T_z$, respectively. The high magnitude of ζ potentials (>30 mV) indicates that both dispersions are colloidally stable. These highly negative ζ potentials are comparable to the values obtained for $Ti_{n+1}C_nT_z$ MXenes and are attributed to the highly functionalized surfaces of the MXenes.[20]

Hydrodynamic diameters were measured using DLS (Figure 2c,d) and determined to be 87.4 and 318 nm for Nb_2CT_z and $Nb_4C_3T_z$, respectively. Because of the anisotropic nature of the MXene nanosheets, these values are not equivalent to the lateral size of the nanosheets. However, previous reports have shown that the hydrodynamic size can be directly correlated to the lateral size from SEM for MXenes and other 2D nanomaterials.[24,25] Maleski et al. utilized a generalized correlation between the hydrodynamic size and the lateral size for a variety of different nanosheet types as shown in eq 2:[25]

$$L = 0.07a_{\mathrm{DLS}}^{1.5} \tag{2}$$

where L is the lateral size and a_{DLS} is the hydrodynamic size from the primary peak. This results in an average lateral size of 57.2 and 397 nm for Nb_2CT_z and $Nb_4C_3T_z$, respectively.

More specifically, a multimodal size distribution was observed for both $Nb_{n+1}C_nT_z$ dispersions. For Nb_2CT_z, three peaks occurred at 13.6 ± 3.0, 139 ± 71, and 4730 ± 760 nm with intensities of 7.1, 91.6, and 1.4%, respectively. In the case of $Nb_4C_3T_z$, three peaks also occurred but at 76.0 ± 23.1, 474 ± 289, and 4430 ± 960 nm with intensities of 12.9, 75.1, and 12.0%, respectively. The leftmost peak is likely due to the formation of small nanosheets after sonication and oxides. Due to the harsh nature of sonication, small nanosheets can easily be broken off. As shown later in this work, MXenes are highly prone to oxidation into their metal oxides which can result in the presence of small particles. The formation of small oxides has been previously confirmed by the in situ formation of TiO_2 nanoparticles when oxidizing $Ti_3C_2T_z$ MXenes.[26,27] Although DLS measurements were taken with fresh MXene dispersions, the low dispersion concentrations (~0.05 mg/mL) necessary for DLS hasten oxidation.[6,20] This is because oxidation actually occurs more quickly at lower concentrations; at high concentration, oxidation is slowed because of intersheet interaction and steric shielding.[20] Additionally, it is possible that some oxidation occurs during the delamination step of MXene synthesis. This is confirmed by XPS of the as-prepared MXenes (Figures S2 and S3) where oxide peaks are observed (~207.5, 210.5 eV). Due to the pore size of the filter paper

https://doi.org/10.1021/acs.jpcc.1c01064
J. Phys. Chem. C 2021, 125, 13990−13996

used for VAF (0.1 μm), it is possible that these smaller particles pass through the filter paper, resulting in their absence in the SEM images. The highest diameter peak is likely due to under-exfoliated MXenes which can be seen as larger particles with an accordion structure in the top-down SEM images (Figure 1d,e). Lastly, the middle peak with the highest intensity is attributed to the desired MXene nanosheets.

After verifying the successful etching of the MXenes, the oxidative stability was then evaluated using UV−vis spectrophotometry. Because MXene concentration has an effect on the rate of oxidation, both MXene dispersions were diluted to the same starting concentration (0.05 mg/mL).[20] Concentration was measured by UV−vis absorbance using extinction coefficients of 1080 and 990 L/g/m for Nb_2CT_z and $Nb_4C_3T_z$, respectively (Figure S4). These extinction coefficients were determined by measuring the absorbance of the MXene dispersions at varying concentrations (Figure S4a,b) and verifying the concentration by VAF. While higher concentrations would result in longer shelf lives, a dispersion concentration of 0.05 mg/mL was used to mitigate the effect of intersheet interaction on the rate of oxidation and ensure dispersion absorbances were low enough to be accurately correlated with the concentration.[20]

To evaluate the effect of low temperature storage and the use of an antioxidant, four samples were prepared for each MXene at the same concentration: with the antioxidant stored at RT (~23 °C), without the antioxidant stored at RT, with the antioxidant stored at 15 °C, and without the antioxidant stored at 15 °C. Absorbance at 776 nm was then measured regularly to evaluate the degree of oxidation (Figure 3). This wavelength was chosen because it is a peak in absorbance for both MXenes (Figure S4a,b). As the MXenes oxidize, their dispersion changes color. The full absorbance spectra as a function of storage time are shown in Figures S5 and S6. The fitting parameters resulting from eq 1 are summarized in Table S3.

In both the cases, the absorbance of the samples that were not treated with an antioxidant plateaued at a much higher absorbance; this indicates that these samples were more prone to oxidation. A plateau occurs when the fraction of the sample that is prone to oxidation has oxidized. This ratio is quantified in Table S1. We then used this metric as a means to compare the oxidative stability of the samples, where a lower oxidizable fraction indicated improved oxidative stability, similar to previous observations of our group when using conductivity as a metric for stability of $Ti_3C_2T_z$.[17]

First, the effect of an antioxidant on the oxidizable fraction was evaluated. When no measures were taken to improve the oxidative stability (e.g., no antioxidant, RT storage), the oxidizable fraction for Nb_2CT_z and $Nb_4C_3T_z$ were 0.62 and 0.51, respectively. When adding the antioxidant, this fraction decreased significantly in both cases to 0.43 and 0.14 for Nb_2CT_z and $Nb_4C_3T_z$, respectively, when stored at RT. This is shown in Figure 3 where the samples with AA show a much higher absorbance plateau than the samples without AA. The significant improvement in oxidizable fraction with the addition of the antioxidant indicates that this is an effective method for improving the oxidative stability of $Nb_{n+1}C_nT_z$ MXenes. The large decrease in the oxidizable fraction is attributed to the antioxidants shielding the edges of the MXene nanosheets. Previous simulation work from our group demonstrated that antioxidants, specifically sodium ascorbate, will associate with the edges of the nanosheets.[17] Because

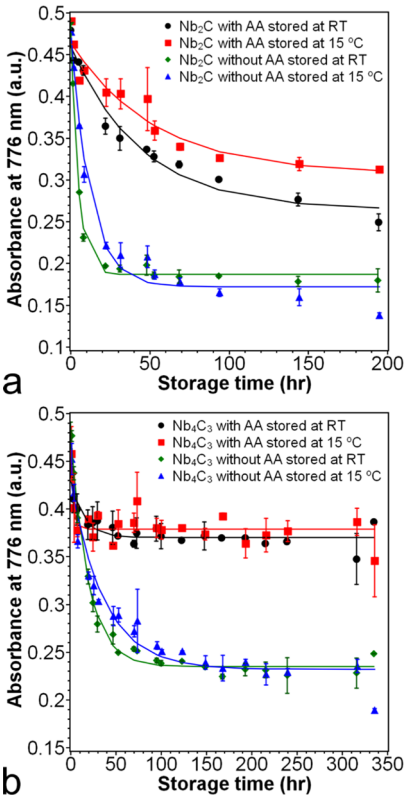

Figure 3. Absorbance at 776 nm at various storage times for (a) Nb_2CT_z and (b) $Nb_4C_3T_z$ dispersions stored under varying conditions. Points represent experimental data. Lines represent a model fit using $A = A_o + A_1 \exp(-t/\tau)$. Absorbance at 776 nm was chosen because it is a peak in absorbance for both MXenes.

oxidation is edge-induced, the antioxidant is able to mitigate oxidation by shielding the edges and preventing the water molecules from interacting with the nanosheet edges.[14] The edge-capping effect was also demonstrated by Natu et al. for $Ti_3C_2T_z$ and V_2CT_z, albeit using polyanionic salts instead, to considerably increase MXene shelf life.[28] Similarly, they attributed this to the polyanion blocking the water molecules and dissolved oxygen from reacting with the nanosheet edges.

Next, the effect of temperature on the oxidative stability was examined. In the case of the samples treated with AA, the samples stored at 15 °C plateaued at a slightly higher value than the samples stored at RT. For the samples stored without AA, the plateau value, A_o, is not significantly different. Looking at the oxidizable fraction, we generally see that the fraction decreases slightly with lower temperature storage. Two exceptions occur with Nb_2CT_z without AA treatment and $Nb_4C_3T_z$ treated with AA. The former is likely due to the samples being highly oxidized without an antioxidant treatment, indicating that the antioxidant is more important for improving the oxidative stability. In the case of $Nb_4C_3T_z$ treated with AA, there is no significant difference between the fractions. Overall, the trend is in agreement with the previous reports on the effect of storage temperature on the oxidative stability for $Ti_3C_2T_z$.[13,14,18] It is expected that further reduction in the storage temperature will result in more pronounced improvements in the oxidative stability of $Nb_{n+1}C_nT_z$ MXenes. This is supported by the work of Zhang et al. who demonstrated improved stability when reducing the storage temperature from RT to 4 °C to −20 °C.[18] This trend

https://doi.org/10.1021/acs.jpcc.1c01064
J. Phys. Chem. C 2021, 125, 13990−13996

with changing temperature is typical of most reactions. As the temperature decreases, the water molecules that induce oxidation will begin to move slower, resulting in it taking longer for those molecules to reach and interact with the MXene nanosheets.

When comparing the oxidative stability of Nb_2CT_z and $Nb_4C_3T_z$, the latter demonstrated a lower oxidizable fraction in all cases. This indicates that MXenes with higher "*n*" are more oxidatively stable. This is in agreement with the previous work from our group comparing the oxidation of $Ti_3C_2T_z$ and Ti_2CT_z.[20] The stability of $Nb_4C_3T_z$ is likely due to the protected inner layers of Nb, in contrast to Nb_2CT_z. The prior literature indicates that surface-terminated Nb-based MXenes, especially −OH terminated, are less stable.[19,29] Because the internal Nb layers of $Nb_4C_3T_z$ are not surface-terminated, they are expected to be more stable. This leads to a higher fraction of the MXene that is less prone to oxidation as compared to Nb_2CT_z. Similarly, prior reports have proposed that MXene oxidation begins at the nanosheet edges; the lower fraction of Nb on the edges and a higher hydrodynamic diameter likely contributes to the higher shelf life as well.[14]

To verify that low temperature storage and the use of an antioxidant improved the oxidative stability, we also used XPS to evaluate how the oxide content of the MXenes changed after aging (Figures 4, S7−S12). In this case, we focused on the two

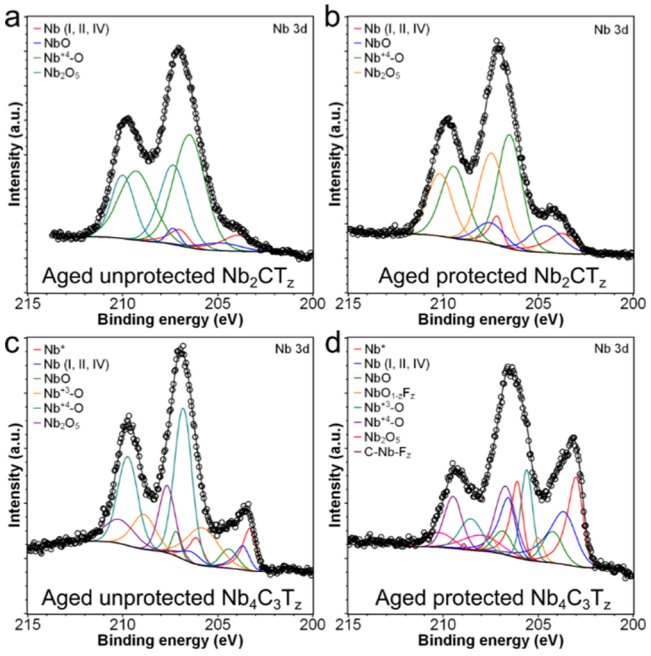

Figure 4. Deconvoluted Nb 3d spectra of (a) unprotected and (b) protected Nb_2CT_z and (c) unprotected and (d) protected $Nb_4C_3T_z$ after aging.

extremes of storage conditions: stored at RT without AA (unprotected) and stored at 15 °C with AA (protected) after 2 weeks of storage. Both MXene dispersions were stored as-prepared without dilution. Concentrations of Nb_2CT_z and $Nb_4C_3T_z$ were ∼3.8 and ∼1.3 mg/mL, respectively. Similar to previous reports, the Nb/O ratio in each case was then compared to the as-prepared MXene dispersion to compare the oxidative stability.[21] In the case of Nb_2C, the Nb/O ratio decreased from 0.63:1 for the as-prepared MXene to 0.52:1 and 0.53:1 for the unprotected and protected Nb_2CT_z, respectively, after aging. The low Nb/O ratio of the as-prepared MXene is indicative of the poor oxidative stability of Nb_2C MXenes, in agreement with the high oxidizable fraction of the samples and is attributed to the oxidation of the MXenes during processing (e.g., intercalation, delamination, and sample preparation). Comparing the two aged samples, a higher Nb/O ratio is observed for the protected sample, supporting that these conditions improve the oxidative stability of Nb_2CT_z. This trend was also observed in the case of $Nb_4C_3T_z$ where the Nb/O ratio of the as-prepared $Nb_4C_3T_z$ decreased from 1.0 to 0.55 and 0.65 for the unprotected and protected $Nb_4C_3T_z$, respectively, after aging.

Because the Nb/O ratio of $Nb_4C_3T_z$ is naturally higher than that of Nb_2CT_z, it is difficult to use this metric to compare the oxidative stability of the two MXenes. As such, we looked at the at % of the specific components in the MXenes. Deconvoluted XPS spectra of the aged samples and the quantified results are shown in Figures 4, S7−S12 and Tables S3−S6. Survey scans (Figures S7 and S10) verified the presence of three major components: Nb, C, and O. As compared to the as-prepared samples, F peaks were either absent or of considerably lower intensity. This is attributed to the oxidation of the −F terminated MXenes. The component spectra from XPS were then deconvoluted to better compare the degree of oxidation of the aged MXene dispersions. The major components used for comparing the degree of oxidation were the various oxides in the Nb 3d spectra, the MXene peak (C−Nb-T_z and Nb-C_v) in the C 1s spectra, and the Nb_2O_5 component in the O 1s spectra. In the case of Nb_2CT_z, the oxides are responsible for 92.2% of the Nb 3d spectra in the as-prepared sample. The high oxide percentage in the as-prepared sample further confirms the poor oxidative stability of Nb_2CT_z. After aging, this percentage increased to 93.5 and 92.5% of the Nb 3d spectra for the unprotected and protected Nb_2CT_z, respectively. Next, the MXene peak in the C 1s spectra was compared to verify that the antioxidant and low temperature storage mitigated the rate of oxidation. For Nb_2CT_z, the C−Nb-T_z and Nb-C_v content in the C 1s spectra was initially 21.4% and decreased to 2.8 and 14.2% for the unprotected and protected Nb_2CT_z dispersions, respectively, after aging. The significantly lower MXene peak in the unprotected Nb_2CT_z dispersion after aging indicates considerable oxidation. In contrast, the MXene peak in the protected Nb_2CT_z dispersion after aging is of considerably higher intensity, confirming that our methods for mitigating oxidation are effective. Lastly, the Nb_2O_5 peak in the O 1s spectra was compared in each case. In this case, the component AT % for the as-prepared Nb_2CT_z dispersion was 27.5% and increased to 84.2 and 72.3% for the unprotected and protected Nb_2CT_z dispersion, respectively, after aging. The stark increase in the Nb_2O_5 component AT % in the O 1s spectra confirms the generally poor oxidative stability of Nb_2CT_z. However, we again verify that the protected Nb_2CT_z dispersion oxidized less than the unprotected Nb_2CT_z dispersion.

We then evaluated the oxidative stability of $Nb_4C_3T_z$ dispersions using XPS (Figures 4c,d, S11 and S12 and Tables S5 and S6). Similar trends are observed in this case where the MXene peaks in the C 1s and Nb 3d component spectra are of significantly lower intensity in the unprotected $Nb_4C_3T_z$ dispersion after aging as compared to the same peaks in the protected $Nb_4C_3T_z$ dispersion after aging. Additionally, as compared to the Nb_2CT_z dispersions after aging, the aged $Nb_4C_3T_z$ dispersions display an improved oxidative stability

https://doi.org/10.1021/acs.jpcc.1c01064
J. Phys. Chem. C 2021, 125, 13990−13996

when comparing dispersions stored under the same conditions. This is evidenced in Figure 4 where the low energy peak of the Nb 3d spectra is of higher intensity in all the cases for the $Nb_4C_3T_z$ samples than in the Nb_2CT_z samples. While the concentrations of the dispersions were different, the $Nb_4C_3T_z$ dispersions were of lower concentration, which is associated with worsened oxidative stability, confirming that $Nb_4C_3T_z$ is more oxidatively stable than Nb_2CT_z.[20]

CONCLUSIONS

In conclusion, the oxidative stability of Nb_2CT_z and $Nb_4C_3T_z$ MXene dispersions was examined. Low-temperature storage, the use of an antioxidant, and higher "*n*" of the MXenes promote oxidation resistance, considerably reducing the oxidizable fraction of the MXene dispersion. The trends in oxidative stability observed in the absorbance measurements were further confirmed by comparing XPS results of the as-prepared and aged dispersions where the aged dispersions were either stored at RT without AA or at 15 °C with AA. By improving the shelf life of $Nb_{n+1}C_nT_z$ MXenes, we open the way for their future use in devices and extend their useful time window for characterization. Further routes to improve the shelf lives of these MXenes include increasing the dispersion concentration, further reducing the storage temperature, evaluating other antioxidants, and using the MXenes in composites.

ASSOCIATED CONTENT

Supporting Information

The Supporting Information is available free of charge at https://pubs.acs.org/doi/10.1021/acs.jpcc.1c01064.

Experimental procedure for MAX phase and MXene synthesis, XPS deconvolution, MXene characterization, XPS survey scans and peak fitting results for as-prepared Nb_2CT_z and $Nb_4C_3T_z$ MXenes, UV−vis spectra and extinction coefficient determination plot for as-prepared Nb_2CT_z and $Nb_4C_3T_z$ MXenes, UV−vis spectra from 300 to 800 nm as a function of storage time for Nb_2CT_z and $Nb_4C_3T_z$ MXene dispersions stored under different conditions, and XPS survey scans and peak fitting results for Nb_2CT_z and $Nb_4C_3T_z$ MXenes after aging (PDF)

AUTHOR INFORMATION

Corresponding Author

Micah J. Green − *Artie McFerrin Department of Chemical Engineering, Texas A&M University, College Station, Texas 77843-3122, United States; Department of Materials Science and Engineering, Texas A&M University, College Station, Texas 77843-3003, United States;* orcid.org/0000-0001-5691-0861; Email: Micah.Green@tamu.edu

Authors

Ian J. Echols − *Artie McFerrin Department of Chemical Engineering, Texas A&M University, College Station, Texas 77843-3122, United States*

Dustin E. Holta − *Department of Materials Science and Engineering, Texas A&M University, College Station, Texas 77843-3003, United States*

Vrushali S. Kotasthane − *Department of Materials Science and Engineering, Texas A&M University, College Station, Texas 77843-3003, United States*

Zeyi Tan − *Department of Materials Science and Engineering, Texas A&M University, College Station, Texas 77843-3003, United States*

Miladin Radovic − *Department of Materials Science and Engineering, Texas A&M University, College Station, Texas 77843-3003, United States*

Jodie L. Lutkenhaus − *Artie McFerrin Department of Chemical Engineering, Texas A&M University, College Station, Texas 77843-3122, United States; Department of Materials Science and Engineering, Texas A&M University, College Station, Texas 77843-3003, United States;* orcid.org/0000-0002-2613-6016

Complete contact information is available at: https://pubs.acs.org/10.1021/acs.jpcc.1c01064

Author Contributions

The manuscript was written through contributions of all authors.

Notes

The authors declare no competing financial interest.

ACKNOWLEDGMENTS

This work was supported by the US National Science Foundation (grant CMMI-1760859) and the Air Force Research Laboratory. Use of the TAMU Materials and Characterization Facility and assistance of Dr. Yordanos Bisrat and Dr. Jing Wu are acknowledged.

ABBREVIATIONS

AA, L-ascorbic acid; DLS, dynamic light scattering; XRD, X-ray powder diffraction; XPS, X-ray photoelectron spectroscopy; SEM, scanning electron microscope; VAF, vacuum-assisted filtration; RT, room temperature; HF, hydrofluoric acid; TBAOH, tetrabutylammonium hydroxide

REFERENCES

(1) Naguib, M.; Kurtoglu, M.; Presser, V.; Lu, J.; Niu, J.; Heon, M.; Hultman, L.; Gogotsi, Y.; Barsoum, M. W. Two-Dimensional Nanocrystals Produced by Exfoliation of Ti3AlC2. *Adv. Mater.* **2011**, *23*, 4248−4253.

(2) Hong, W.; Wyatt, B. C.; Nemani, S. K.; Anasori, B. Double transition-metal MXenes: Atomistic design of two-dimensional carbides and nitrides. *MRS Bull.* **2020**, *45*, 850−861.

(3) Ling, Z.; Ren, C. E.; Zhao, M.-Q.; Yang, J.; Giammarco, J. M.; Qiu, J.; Barsoum, M. W.; Gogotsi, Y. Flexible and conductive MXene films and nanocomposites with high capacitance. *Proc. Natl. Acad. Sci. U.S.A.* **2014**, *111*, 16676−16681.

(4) An, H.; Habib, T.; Shah, S.; Gao, H.; Patel, A.; Echols, I.; Zhao, X.; Radovic, M.; Green, M. J.; Lutkenhaus, J. L. Water Sorption in MXene/Polyelectrolyte Multilayers for Ultrafast Humidity Sensing. *ACS Appl. Nano Mater.* **2019**, *2*, 948−955.

(5) Zhou, Z.; Panatdasirisuk, W.; Mathis, T. S.; Anasori, B.; Lu, C.; Zhang, X.; Liao, Z.; Gogotsi, Y.; Yang, S. Layer-by-layer assembly of MXene and carbon nanotubes on electrospun polymer films for flexible energy storage. *Nanoscale* **2018**, *10*, 6005−6013.

(6) Echols, I. J.; An, H.; Zhao, X.; Prehn, E. M.; Tan, Z.; Radovic, M.; Green, M. J.; Lutkenhaus, J. L. pH-Response of polycation/Ti3C2Tx MXene layer-by-layer assemblies for use as resistive sensors. *Mol. Syst. Des. Eng.* **2020**, *5*, 366−375.

(7) Yun, J.; Echols, I.; Flouda, P.; Wang, S.; Easley, A.; Zhao, X.; Tan, Z.; Prehn, E.; Zi, G.; Radovic, M.; Green, M. J.; Lutkenhaus, J. L. Layer-by-Layer Assembly of Polyaniline Nanofibers and MXene Thin-Film Electrodes for Electrochemical Energy Storage. *ACS Appl. Mater. Interfaces* **2019**, *11*, 47929−47938.

(8) Han, M.; Shuck, C. E.; Rakhmanov, R.; Parchment, D.; Anasori, B.; Koo, C. M.; Friedman, G.; Gogotsi, Y. Beyond Ti3C2Tx: MXenes for Electromagnetic Interference Shielding. *ACS Nano* **2020**, *14*, 5008−5016.
(9) Maleski, K.; Shuck, C. E.; Fafarman, A. T.; Gogotsi, Y. The Broad Chromatic Range of Two-Dimensional Transition Metal Carbides. *Adv. Opt. Mater.* **2021**, *9*, 2001563.
(10) Halim, J.; Persson, I.; Moon, E. J.; Kühne, P.; Darakchieva, V.; Persson, P. O. Å.; Eklund, P.; Rosen, J.; Barsoum, M. W. Electronic and optical characterization of 2D Ti2C and Nb2C (MXene) thin films. *J. Phys.: Condens. Matter* **2019**, *31*, 165301.
(11) Su, T.; Peng, R.; Hood, Z. D.; Naguib, M.; Ivanov, I. N.; Keum, J. K.; Qin, Z.; Guo, Z.; Wu, Z. One-Step Synthesis of Nb2O5/C/Nb2C (MXene) Composites and Their Use as Photocatalysts for Hydrogen Evolution. *ChemSusChem* **2018**, *11*, 688−699.
(12) Zhao, S.; Meng, X.; Zhu, K.; Du, F.; Chen, G.; Wei, Y.; Gogotsi, Y.; Gao, Y. Li-ion uptake and increase in interlayer spacing of Nb4C3 MXene. *Energy Storage Mater.* **2017**, *8*, 42−48.
(13) Habib, T.; Zhao, X.; Shah, S. A.; Chen, Y.; Sun, W.; An, H.; Lutkenhaus, J. L.; Radovic, M.; Green, M. J. Oxidation stability of Ti3C2Tx MXene nanosheets in solvents and composite films. *npj 2D Mater. Appl.* **2019**, *3*, 8.
(14) Zhang, C. J.; Pinilla, S.; McEvoy, N.; Cullen, C. P.; Anasori, B.; Long, E.; Park, S.-H.; Seral-Ascaso, A.; Shmeliov, A.; Krishnan, D.; Morant, C.; Liu, X.; Duesberg, G. S.; Gogotsi, Y.; Nicolosi, V. Oxidation Stability of Colloidal Two-Dimensional Titanium Carbides (MXenes). *Chem. Mater.* **2017**, *29*, 4848−4856.
(15) Lee, Y.; Kim, S. J.; Kim, Y.-J.; Lim, Y.; Chae, Y.; Lee, B.-J.; Kim, Y.-T.; Han, H.; Gogotsi, Y.; Ahn, C. W. Oxidation-resistant titanium carbide MXene films. *J. Mater. Chem. A* **2020**, *8*, 573−581.
(16) Lotfi, R.; Naguib, M.; Yilmaz, D. E.; Nanda, J.; van Duin, A. C. T. A comparative study on the oxidation of two-dimensional Ti3C2MXene structures in different environments. *J. Mater. Chem. A* **2018**, *6*, 12733−12743.
(17) Zhao, X.; Vashisth, A.; Prehn, E.; Sun, W.; Shah, S. A.; Habib, T.; Chen, Y.; Tan, Z.; Lutkenhaus, J. L.; Radovic, M.; Green, M. J. Antioxidants Unlock Shelf-Stable Ti3C2T (MXene) Nanosheet Dispersions. *Matter* **2019**, *1*, 513−526.
(18) Zhang, J.; Kong, N.; Hegh, D.; Usman, K. A. S.; Guan, G.; Qin, S.; Jurewicz, I.; Yang, W.; Razal, J. M. Freezing Titanium Carbide Aqueous Dispersions for Ultra-long-term Storage. *ACS Appl. Mater. Interfaces* **2020**, *12*, 34032−34040.
(19) Zhao, X.; Holta, D. E.; Tan, Z.; Oh, J.-H.; Echols, I. J.; Anas, M.; Cao, H.; Lutkenhaus, J. L.; Radovic, M.; Green, M. J. Annealed Ti3C2Tz MXene Films for Oxidation-Resistant Functional Coatings. *ACS Appl. Nano Mater.* **2020**, *3*, 10578−10585.
(20) Zhao, X.; Vashisth, A.; Blivin, J. W.; Tan, Z.; Holta, D. E.; Kotasthane, V.; Shah, S. A.; Habib, T.; Liu, S.; Lutkenhaus, J. L.; Radovic, M.; Green, M. J. pH, Nanosheet Concentration, and Antioxidant Affect the Oxidation of Ti 3 C 2 T x and Ti 2 CT x MXene Dispersions. *Adv. Mater. Interfaces* **2020**, *7*, 2000845.
(21) Palisaitis, J.; Persson, I.; Halim, J.; Rosen, J.; Persson, P. O. Å. On the Structural Stability of MXene and the Role of Transition Metal Adatoms. *Nanoscale* **2018**, *10*, 10850−10855.
(22) Halim, J.; Cook, K. M.; Naguib, M.; Eklund, P.; Gogotsi, Y.; Rosen, J.; Barsoum, M. W. X-ray photoelectron spectroscopy of select multi-layered transition metal carbides (MXenes). *Appl. Surf. Sci.* **2016**, *362*, 406−417.
(23) Ghidiu, M.; Naguib, M.; Shi, C.; Mashtalir, O.; Pan, L. M.; Zhang, B.; Yang, J.; Gogotsi, Y.; Billinge, S. J. L.; Barsoum, M. W. Synthesis and characterization of two-dimensional Nb4C3 (MXene). *Chem. Commun.* **2014**, *50*, 9517−9520.
(24) Lotya, M.; Rakovich, A.; Donegan, J. F.; Coleman, J. N. Measuring the lateral size of liquid-exfoliated nanosheets with dynamic light scattering. *Nanotechnology* **2013**, *24*, 265703.
(25) Maleski, K.; Ren, C. E.; Zhao, M.-Q.; Anasori, B.; Gogotsi, Y. Size-Dependent Physical and Electrochemical Properties of Two-Dimensional MXene Flakes. *ACS Appl. Mater. Interfaces* **2018**, *10*, 24491−24498.
(26) Zhang, J.; Yang, L.; Wang, H.; Zhu, G.; Wen, H.; Feng, H.; Sun, X.; Guan, X.; Wen, J.; Yao, Y. In Situ Hydrothermal Growth of TiO2 Nanoparticles on a Conductive Ti3C2Tx MXene Nanosheet: A Synergistically Active Ti-Based Nanohybrid Electrocatalyst for Enhanced N2 Reduction to NH3 at Ambient Conditions. *Inorg. Chem.* **2019**, *58*, 5414−5418.
(27) Li, N.; Jiang, Y.; Zhou, C.; Xiao, Y.; Meng, B.; Wang, Z.; Huang, D.; Xing, C.; Peng, Z. High-Performance Humidity Sensor Based on Urchin-Like Composite of Ti3C2 MXene-Derived TiO2 Nanowires. *ACS Appl. Mater. Interfaces* **2019**, *11*, 38116−38125.
(28) Natu, V.; Hart, J. L.; Sokol, M.; Chiang, H.; Taheri, M. L.; Barsoum, M. W. Edge Capping of 2D-MXene Sheets with Polyanionic Salts To Mitigate Oxidation in Aqueous Colloidal Suspensions. *Angew. Chem., Int. Ed.* **2019**, *58*, 12655−12660.
(29) Fu, Z. H.; Zhang, Q. F.; Legut, D.; Si, C.; Germann, T. C.; Lookman, T.; Du, S. Y.; Francisco, J. S.; Zhang, R. F. Stabilization and strengthening effects of functional groups in two-dimensional titanium carbide. *Phys. Rev. B* **2016**, *94*, 104103.

https://doi.org/10.1021/acs.jpcc.1c01064
J. Phys. Chem. C 2021, 125, 13990−13996